Solar Energy Materials & Solar Cells 150 (2016) 10–18

Contents lists available at ScienceDirect

Solar Energy Materials & Solar Cells

journal homepage: www.elsevier.com/locate/solmat

Morphological control and performance improvement of organic photovoltaic layer of roll-to-roll coated polymer solar cells

Yu-Ching Huang *,[1], Hou-Chin Cha [1], Charn-Ying Chen, Cheng-Si Tsao

Institute of Nuclear Energy Research, Taoyuan 32546, Taiwan

ARTICLE INFO

Article history:
Received 1 November 2015
Received in revised form
17 January 2016
Accepted 30 January 2016
Available online 15 February 2016

Keywords:
Slot-die
Morphology
Thermal treatment
Crystallization
Phase transformation

ABSTRACT

We systematically investigated the thermal effects of drying process as well as thermal annealing on morphology and performance of inverted polymer solar cells (PSCs) fabricated by roll-to-roll (R2R) slot-die coating. Power conversion efficiency (PCE) of PSCs layer is strongly influenced by bulk heterojunction (BHJ) active layer. Compared to the conventional annealing process, we demonstrate that the drying process for transforming the wet active layer into solid-state film (an early polymer crystallization step) in the R2R process is a critical control of morphological evolution to the desired structure. We have demonstrated that a significant improvement in performance of inverted PSCs can be achieved by tuning the parameters in the drying process prior to the annealing process. This study provides the mechanistic understanding of how the drying and annealing processes affect the morphological evolution regarding to the crystallinity, BHJ structure and interface between layers. Moreover, with respect to environmental concerns, halogen-free are carried out as an alternative solvent to halogenated solvents. We successfully incorporate halogen-free solvent, o-xylene, with an elevated drying temperature for improving the performance of R2R slot-die coated inverted solar cells.

1. Introduction

Polymer solar cells (PSCs) have attracted tremendous attention over the past decade and have been deemed to a promising photovoltaic technology due to their benefits such as light weight, low manufacturing cost, and compatibility with flexible and large-area applications [1–3]. The power conversion efficiency (PCE) of PSCs with a single bulk heterojunction (BHJ) structure consisted of conducting polymers as electron donor materials blended with fullerene derivatives as electron acceptor materials has been achieved 8–10% [4,5]. Furthermore, the PCE of PSCs has reached more than 10% with a multijunction structure, such as tandem and triple-junction PSCs [6–9]. With the rapid growth of PSCs′ performance, many researching groups have focused on the field related to the commercialization of PSCs in recent years, for instance device stability [10–12] and large-area fabrication [1,13–17]. An inverted structure has been studied extensively to obtain a long device operation time [18]. In the inverted PSCs, the charges drift to opposite electrodes in comparison with conventional PSCs. Therefore, inverted PSCs allow the use of high work function metals as top electrode, such as Ag and Au, which are less air-sensitive. In addition, an electron transport layer (ETL), such as zinc oxide (ZnO) [19] and caesium carbonate (Cs_2CO_3) [20], is used to cover on the transparent indium tin oxide (ITO) electrode, to replace poly(3,4-ethylenedioxythiophene):poly(styrenesulfonate) (PEDOT:PSS) to prevent from etching ITO electrode due to the acidic nature of PEDOT:PSS.

Large-area coating of PSCs have been developed to facilitate the mass production, such as spray [14,21], inkjet printed [22], gravure printing [23,24], slot-die and screen printing processes [25–28]. One of the most attractive advantages of PSCs is the high mechanical flexibility that is suitable for roll-to-roll (R2R) processing technique. The R2R processing technique has been used to fabricate PSCs due to its fast process [1,29]; however, it is still challenging to achieve a high PCE. Among these processes, slot-die coating is the most widely used in the R2R process for the large-area production of PSCs due to its reproducibility, high coating quality and high throughput. Recently, several studies have been demonstrated the ability to fabricate large-area PSCs by slot-die coating [17,26,30–34]. Although substantial studies have been performed on the development of conventional PSCs fabricated by slot-die process, the high-efficiency inverted slot-die-coated PSCs are still critically lacking [35,36]. The literature pointed out that the PCE of PSCs layer is strongly influenced by BHJ active layer or polymer crystallinity [37–42]. The BHJ structure is a phase-separated interpenetration network and can be tailored by various treatments, such as thermal annealing [37], addition of

* Corresponding author.
E-mail address: huangyc@iner.gov.tw (Y.-C. Huang).
[1] These authors contributed equally to this work.

http://dx.doi.org/10.1016/j.solmat.2016.01.042
0927-0248/

nanoparticles [38], change of acceptor components [39,40] and additive [42]. The BHJ structure can also be tailored by the radical oxidation with nitrogen plasma treatment [43]. The plasma treatment can provide the high energy of ions diffusing into the surface layer to produce the high-area surface and serve as the defects/doping inside the structure (inducing the other reactions to form local BHJ structure). In comparison with the spin-coating process, the slot-die coating process is a relatively slow thin-film formation and then crystal growth process. The films fabricated by spin coating are usually dried in a few seconds because the substrate is rotated at high speed. However, the drying rate and drying temperature of the films deposited by the slot-die or blade coating could cause a different mechanism (P3HT crystallization and PCBM aggregation) during drying process from wet film to dry film, which influence the subsequently thermal annealing effect [44]. Many factors affect the drying process, such as the mass solvent of the coating materials, solution concentration, deposit amount of the solution and coating rate. Therefore, we can optimize the performance of slot-die coated devices by controlling the film formation and the subsequent crystallization growth more effectively, but such a manuscript cannot be conducted in the spin coat process. Basically, few studies [17,45] reported how to thermally tailor BHJ structure in the R2R slot-die coating process different from the well-known annealing treatment for spin-coating process.

In this study, high-efficiency inverted PSCs consisted of the blends of poly(3-hexylthiophene) (P3HT) and [6,6]-phenyl C_{61} butyric acid methyl ester (PCBM) were fabricated by R2R slot-die coating process. The past researches only focused on the effect of conventionally thermal annealing on the performance. There are very few studies demonstrating how the drying process as the first pre-treatment affects the performance. We illustrated herein that the control of the drying process from wet film to dry film plays an important role in tailoring the device performance; even these P3HT/PCBM dry films were treated with the same thermal annealing process. We also investigated the factors, including the drying temperature for solidification of wetly coated film into dry film (control of the early crystallization), determining the performance of inverted PSCs, absorption behavior and nanostructure evolution. Our results show an improvement in performance of inverted PSCs coated at a high drying temperature of 110 °C. Halogenated solvents, such as chloroform (CF), chlorobenzene (CB) and 1,2-dichlorobenzene (DCB), are widely used as the host solvent of photoactive layer due to the high solubility. However, halogenated solvents are not acceptable in the mass production because of their toxicity, corrosive property and environmental concerns. In recent, halogen-free solvents are studied for an alternative to halogenated solvents [46]. In this study, we successfully incorporated halogen-free solvent, o-xylene, in the slot-die coating process and obtained an equivalent performance to that of PSCs fabricated by halogenated solvents.

2. Experimental

2.1. Materials

The ITO-coated polyethylene terephthalate (PET) substrate was purchased from Optical Filters Ltd (EMI-ito 15, surface resistance of 15 Ω/square). Zinc acetate and aluminum acetate were obtained from Alfa Aesar and Aldrich, respectively. The surfactant Zonyl FS-300 was purchased from Fluka. Polyethylenimine ethoxylated (PEIE) received from Aldrich was diluted in 2-methoxyethanol into 0.4 wt% of solution. We prepared the precursor of aluminum doped zinc oxide (AZO) solution by dissolving zinc acetate (1 g), aluminum acetate (0.015 g) and Zonyl FS-300 (0.06 g) in 10 g of deionized water (DIW). The as-prepared AZO precursor was filtered through a 0.45 μm filter, and then diluted with DIW by the volume ratio of 1:1. After that, the AZO precursor was mixed with 20 vol% of PEIE to form a hybrid solution of AZO:$PEIE_{20}$. P3HT (MW∼35,000, PDI and RR are ∼2 and 90%, respectively) and PCBM were provided by Rieke Metals. We prepared the active layer solution by dissolving 12 mg of P3HT and 12 mg PCBM in 1 ml chlorobenzene (CB) or o-xylene solution.

2.2. R2R slot-die coating process for PSC fabrication

We slot-die coated the ETL and photoactive layer by using Coatema R2R system (Coatema smartcoater, Germany). Because our laboratory-scale R2R equipment is not suitable for full-R2R process, the PET/ITO substrate was cut into 10×10 cm^2 and it was spliced in the machine. The widths of web and slot-die coater are 14.2 and 10 cm, respectively. All the coating speed used for each layer is 1 m/min. The solution output rates for ETL and active layer are 0.8 and 1.2 ml/min, respectively, using a mask of 100 μm thickness. Prior to the ETL deposition, the flexible ITO-coated PET substrate was treated with air plasma at the web speed of 1 m/min. The experimental procedure, photographs of Coatema R2R system and device structure were described previously [25]. There are two ovens we used here. One oven with a length of 50 cm is installed in the R2R system for drying the active layer from wet film to dry film. We called it as R-oven. The other one, called A-oven, is set in ambient atmosphere. To stably keep the temperatures of ovens, we pre-heated these ovens for 40 min before testing. For the photovoltaic devices fabrication, we dried the deposited ETL at 150 °C for 10 min in the A-oven. The deposited wet active layer was dried at various temperatures in the R-oven, and then thermal annealed (TA) at 130 °C for 10 min in the A-oven. The dried thicknesses of ETL and active layer are about 60 and 150 nm, respectively. We thermally evaporated hole transport layer (HTL) of MoO_3 and silver electrode on the active layer in a separate thermal evaporator. The thicknesses of MoO_3 and silver were 5 nm and 100 nm, respectively. The structure of the devices is PET/ITO/ETL/active layer/MoO_3/Ag. The device area is defined by the metal electrode with the area of 1×0.3 cm^2. It is noteworthy to mention that all the R2R coating processes were conducted in air.

2.3. Performance measurement and structural characterization

Current density–voltage curves were measured by using a solar simulator (Abet technologies, Model # 11,000) under A.M. 1.5 illumination (100 mW/cm^2) and ambient condition. All slot-die coated layers for the relevant tests were fabricated in the same batch, and the devices were not encapsulated. The thicknesses of films were measured by a profilometer (Alpha Step D-100, KLA Tencor). Surface roughness and morphology of the blend films were analyzed by atomic force microscopy (AFM, Digital Instruments, Nanoscope III). The UV–vis absorption and photoluminescence (PL) spectra of the P3HT:PCBM films were obtained using a UV–vis spectrometer (Perkin Elmer Lambda 35) and a spectrofluorometer (Perkin Elmer FS-55). The R_s and R_{sh} of PSCs were evaluated based on the measured J–V curves.

3. Results and discussion

Nanomorphology of photoactive layer plays a critical role in its performance. In the R2R slot-die coating process, the BHJ nanomorphology is strongly influenced by the thermal effects of two steps: (1) drying process to evaporate the solvent for forming the solid-state film (i.e., early polymer crystallization) and

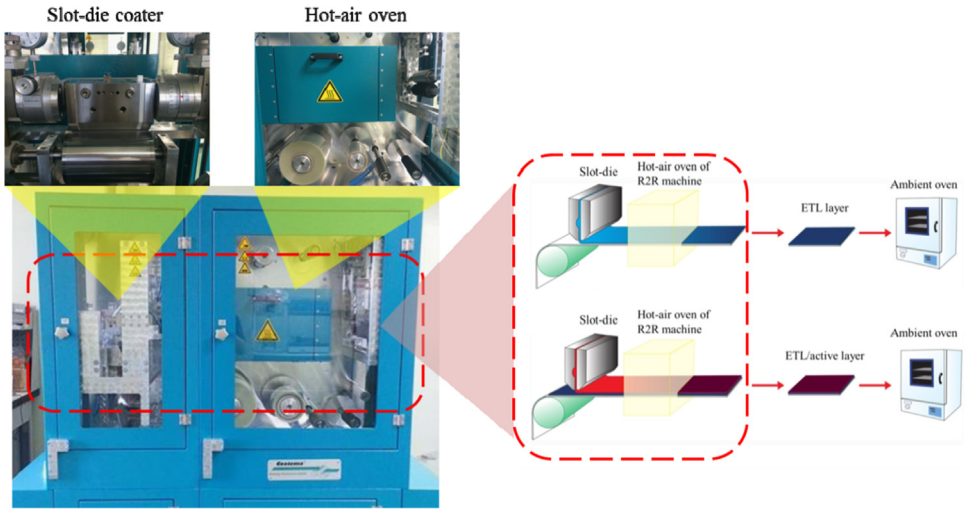

Fig. 1. Left panel: picture of laboratory-scale R2R equipment. Right panel: diagram of sequential ETL and active layer deposition on the ITO/PET substrate by slot-die coating process.

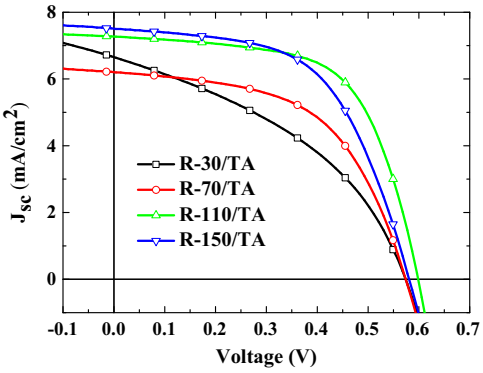

Fig. 2. *J–V* curves of devices based on the active layers prepared with chlorobenzene as host solvent and drying temperatures of 30, 70, 110 and 150 °C.

(2) annealing process to form the appropriate BHJ nanomorphology (i.e., development of complete polymer crystallization). Previous literature [47] using spin-coat process to prepare active layers indicated that the rapid film growth results in a low PCE. In contrast, the formation mechanism of R2R coated film is more complex due to the two-step crystallization. The nucleation and initial growth of crystalline film during the drying process (in the R-oven) could influence the quality of late crystallization in the subsequently annealing process. Few studies reported the effect of drying process on the performance and morphological control [44,45,48,49].

Considering the different formation mechanism of the R2R coated film from that of spin-coated film, we first present a systematic study of the effect of drying temperature on the PCE of devices manufactured by R2R process. Fig. 1 shows our laboratory-scale R2R picture and slot-die coating process, and the device structure is PET/ITO/ETL/active layer/MoO_3/Ag. We slot-die coated the photoactive layer on a PET/ITO substrate covered with ETL (AZO:$PEIE_{20}$) at the speed of 1 m/min. The active layer was immediately treated with different drying temperatures of 30, 70, 110 and 150 °C by the sequence oven (R-oven) equipped on R2R machine. We named these films prepared with the above drying temperatures as R-30, R-70, R-110 and R – 150, respectively. These thermally drying treatments result in a different solid-film growth rate. For instant, active layer treated with 150 °C (R-150) was dried faster than that with 30 °C. We fabricated photovoltaic devices based on these dry films with a further thermally annealing process at 130 °C for 10 min, and we named the devices as R-X/TA, which X is the drying temperature of R-oven. Fig. 2 shows that the *J–V* curves of P3HT:PCBM PSC devices based on different drying temperatures. The photovoltaic properties are summarized in Table 1. Compared to the R-30/TA device (as reference device) with a PCE of 1.93%, the R-70/TA device shows a similar PCE (1.94%). The highest PCE of 2.69% is achieved for the R-110/TA device, which is ~37% of enhancement in PCE compared to that of reference device. Upon increasing R2R oven temperature to 150 °C, the PCE of R-150/TA device reduces to 2.46%, which still has ~27% PCE of enhancement as compared to that of the reference device. Obviously, the P3HT:PCBM films treated with relatively high drying temperatures (110 and 150 °C) show a great enhancement in PCEs. We found that the enhanced PCEs result from the improved fill factor, which implies a reducing charge recombination and loss. To develop the non-toxic process by using halogen-free solution, we adopted o-xylene as the host solvent of active layer instead of CB. The abovementioned experimental condition was repeated for the use of o-xylene. The *J–V* curves are shown in Fig. 3, and the corresponding performances are listed in Table 2. The PCE trend is the same as the abovementioned results. A remarkable PCE of 2.80% was achieved as the drying temperature is set at 110 °C. The PCE slightly reduces to 2.73% as the drying temperature reaches to 150 °C. According to these results, we confirm that (1) o-xylene is a good alternative host solvent compared to CB, and (2) a suitable drying treatment is critical for the photoactive layer deposited by slot-die coating.

Previous literature [47] pointed out that at elevated temperature the P3HT:PCBM film loses its crystallinity due to a rapid solvent removal. A reduction in PCE resulted from the low polymer crystallinity. However, these devices were fabricated by spin-coating process; our PCE results based on R2R-coated devices had different trend. We measured the absorption behavior of the R2R-coated P3HT:PCBM films by UV–vis spectroscopy and the spectra are shown in Fig. 4. The absorption spectra were normalized by the related film thickness, and the absorption peak at 480 nm is due to the contributions of P3HT. The absorption intensity results from the π–π stacking ordering of the P3HT chain [50]. The absorption peak intensity of P3HT:PCBM films decreases with the increase of R-oven's drying temperature. The reduction of absorption indicates a decreasing crystallinity of the blend films. This result is consistent with previous literature data. The crystallinity of P3HT:PCBM films was enhanced with a further thermal annealing at 130 °C for 10 min (i.e., complete-crystallization step)

Table 1
Photovoltaic characterization of devices under various thermal treatments by R2R oven. The photoactive layer of these devices was obtained from host solvent of chlorobenzene. The device area is 0.3 (1×0.3) cm^2, and the data are averaged over 20 devices.

Treatment	J_{sc} (mA/cm^2)	V_{oc} (V)	FF (%)	PCE_{avg} (%)	PCE_{best} (%)
R-30	7.340 ± 0.623	0.575 ± 0.004	40.1 ± 1.9	1.69 ± 0.21	1.93
R-70	6.762 ± 0.602	0.570 ± 0.010	45.3 ± 7.9	1.72 ± 0.18	1.94
R-110	7.054 ± 0.402	0.591 ± 0.004	59.7 ± 1.5	2.49 ± 0.15	2.69
R-150	7.551 ± 0.040	0.582 ± 0.008	55.5 ± 0.7	2.44 ± 0.03	2.46

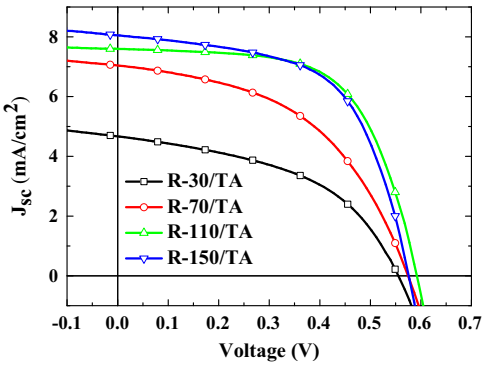

Fig. 3. *J–V* curves of devices based on the active layers prepared with o-xylene as host solvent and drying temperatures of 30, 70, 110 and 150 °C.

[40]. Nevertheless, the R-30/TA film exhibits the highest absorption (i.e., the highest crystallinity). It indicates that the nucleation and initial growth kinetics in the drying process govern the final crystallization quality. The development of crystallization in the annealing process only plays an auxiliary role [43], being subject to the structure produced by drying (will be examined in the subsequent work). Therefore, the slow-drying control at 30 °C provides the enough time to form relatively large crystallites during solvent removal, leading to the highest crystallinity via the annealing process. Apparently, the performance of R2R devices was not explained by the absorption spectrum and crystallinity. There should be other factors influenced the performance of the R2R-coated devices. Moreover, Fig. 5 shows the PL spectra of R-30/TA and R-110/TA films to compare the PL quenching, which provided useful information on the charge separation and transport at the interface between P3HT and the PCBM phases. The PL quenching efficiencies of R-30/TA and R-110/TA films as compared with the PL intensity of pristine P3HT film are calculated to be 74% and 96%, respectively. The R-30/TA film shows a decreasing PL quenching ability, which indicated that a lower charge separation and transport takes place, and suggests the fewer interface area between P3HT and PCBM (more aggregation), although the UV–vis absorption of R-30 film/TA is slightly higher than that of R-110/TA film. This result and following AFM results support the interpretation to the increasing J_{sc} of the R-110/TA devices.

According to our previous research [25], the AZO:$PEIE_{20}$ film as ETL coated by R2R process exhibited a high roughness of 12.9 nm. Surface morphologies of the photoactive films treated with R-oven (drying process) were studied by atomic force microscopy (AFM) in tapping mode (Fig. 6), and the root-mean-square (RMS) roughness of these films were calculated by the AFM software. The surface morphology of the reference photoactive film, R-30, (Fig. 6a) shows an obvious stripe-like topography with a RMS roughness of 4.2 nm. Surface roughness of the slot-die coated P3HT:PCBM films represented the interfacial contact between active layer and electron transport layer. Moreover, the low surface roughness of active layer also implied an improved interfacial contact between the active layer and MoO_3/Ag anode. A smooth film surface was obtained after the deposition of photoactive film on ETL. However, the morphology of P3HT:PCBM film was still strongly affected by the underneath layer surface when the photoactive film dried slowly. With a further thermal annealing, we can obtain a smooth surface of photoactive film with a RMS roughness of 2.6 nm (Fig. 6d). The reduction in roughness after thermal annealing implies that there is a good interfacial contact between photoactive layer and ETL. Fig. 6b demonstrated the surface morphology of R-110 photoactive films. It shows a flat uniform surface with a RMS roughness of 1.8 nm. After the further thermal annealing, a similar RMS roughness of 2.0 nm was observed (Fig. 6e), indicating that the as-cast photoactive film dried by R-oven at 110 °C has exhibited a good interfacial contact between photoactive layer and ETL. It is well-known that the interfacial contact among electron transport layer (ETL), active layer and metal electrode play a critical role in the charge extraction efficiency. The good contact is partly represented by the smooth surface morphology on the ETL measured by AFM topography (i.e., uniform interfacial contact between the ETL and the active layer). Moreover, the quality of good contact between layers can be measured by the low series resistance (R_s) and high fill factor, as reported by the literatures [51,52]. Fig. 6c and f show the morphologies of R-150 photoactive film before and after thermal anneal respectively. They are consistent with R – 110 films. The plane surfaces of R-110/TA and R-150/TA films also inferred a good contact between photoactive layer and metal electrode, and it would result in an effective charge collecting and enhanced performance. The morphologies formed in the drying process (Fig. 6a, b and c) are similar to those formed in the subsequent thermal annealing process (Fig. 6d, e and f), showing the drying process is the critical step to control the final morphology for the R2R slot-die coated film, and thus affect the performance of photovoltaics.

On the other hand, the observed morphologies show the characteristics of different BHJ active layer structures tailored by the drying process discussed as follows. The large stripe-like P3HT-rich domain formed by the slow drying at 30 °C (Fig. 6a) imply a high degree of phase-separation BHJ structure. This structure may have good paths for charge carrier transport but has the lowest interface area between the P3HT phase and PCBM phase (clusters) [39,53]. The latter could cause the poor capacity of separation for charge carriers. In contrast, the fine or small polymer crystallites formed by the quick drying at high temperature (>100 °C; Fig. 6b and c) demonstrate the well intermixing between nanoscale P3HT and PCBM phases. It indicates that the interface area between the P3HT phase and PCBM phase is very large, leading to a high efficiency of separation for charge carriers and thus performance improvement (increase of short-circuit current in Table 2). This interpretation would be supported by the measurement of resistance discussed later. In conclusion, the best performance resulted by the drying at 110 °C is contributed by the trade-off among the crystallinity, favorable BHJ active layer structure and interface effect between layers.

To further confirm this hypothesis about the morphological control, we heated a photoactive films based on the o-xylene solvent in an ambient oven (A-oven) at 70, 110 and 150 °C for 30 s. We named these films as A-70, A-110 and A-150. These films are almost-dried at room temperature in the R-oven; afterwards, they

Table 2
Photovoltaic characterization of devices under various thermal treatments by R2R oven. The photoactive layer of these devices was obtained from host solvent of o-xylene. The device area is 0.3 (1×0.3) cm^2, and the data are averaged over 20 devices.

Treatment	J_{sc} (mA/cm^2)	V_{oc} (V)	FF (%)	PCE$_{avg}$ (%)	PCE$_{best}$ (%)
R-30	4.876 ± 0.17	0.534 ± 0.02	44.667 ± 2.45	1.16 ± 0.072	1.22
R-70	7.198 ± 0.208	0.569 ± 0.006	46.9 ± 1.513	1.92 ± 0.03	1.95
R-110	7.683 ± 0.076	0.584 ± 0.007	60.7 ± 1.353	2.723 ± 0.068	2.8
R-150	8.096 ± 0.076	0.573 ± 0.002	56.567 ± 2.155	2.627 ± 0.093	2.73

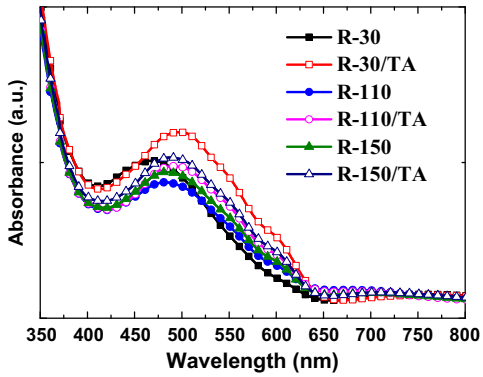

Fig. 4. Absorption spectra of active layers prepared with (1) the drying process at different temperatures and (2) two-step process (drying and thermal annealing).

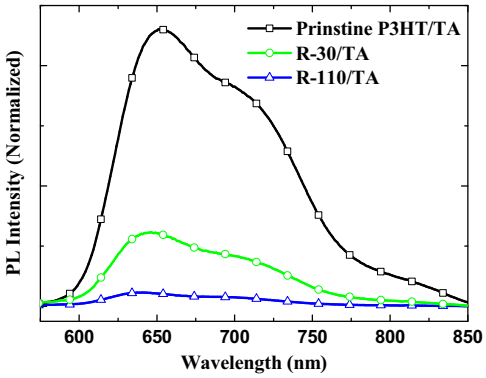

Fig. 5. PL spectra of pristine annealed P3HT film, annealed P3HT:PCBM films pretreated with R2R oven (R-oven) at 30 °C (R-30/TA) and 110 °C (R-110/TA).

were transferred to the A-oven. It means that the photoactive film is almost dried before the thermal heating at the A-oven. The corresponding *J–V* curves and photoelectric characteristics are shown and summarized in Fig. 7 and Table 3, respectively. Interestingly, for the A-series devices with the same drying process, the similar PCEs (~1.3%) were observed for the annealing temperatures ranging from 70 to 150 °C. The unchanged fill factor was observed in these devices. In comparison with the previous results shown in Fig. 3, it is worth noting that the immediate heating process treated on the wet film plays a more important role than that treated on the dried film. Furthermore, the AFM images of A-series films (A-110 and A-150) were shown in Fig. 8a and b, and these films exhibit a similar morphology to reference P3HT:PCBM film (R-30). The morphologies of these films with a further thermal annealing process (Fig. 8c and d) are close to those presented in Fig. 8a and b. These results also support the above-mentioned argument that the drying process is dominated to the morphology for the R2R slot-die coated film. Both A-110 and R-110 were almost treated with the same thermal energy at 110 °C. The only difference was that the R-110 film treated at the initial stage of film formation, i.e. from solution-state film to dry film, but the A−110 film fully treated at the dry film. However, the morphology and performance of the devices based on these two films were largely different (2.69% for R-110/TA and 1.38% for A-110/TA). Additionally, the R-110 device shows a lower R_s than that of A-110 device, and the low R_s of R-110 device results from a good interfacial contact between photoactive layer and evaporated metal electrode. The shunt resistance (R_{sh}), which is related to the charge carriers recombination or the charge separation at the donor/acceptor interface, of R-110 device was 2–3 order of magnitude larger than that of A-110 device. These results indicate that the good photoelectric properties of R- series devices, such as low R_s and high R_{sh} values, are contributed to the improvement of PCE. This result remarkably demonstrated the thermal treatment during the initial stage of film formation (or drying process) from wet film to dry film is the most critical to the device performance.

To support the claim of the better intermixing between P3HT and PCBM phases, Fig. 9 presented the topographic and phase images of R-30, R-110 and A-110 films. The AFM phase image of the blend film treated with inline oven (R-oven) at 110 °C still showed the well phase-separated and similar contrast compared to the corresponding topography image. It suggests that phase mode can reflect the measure of phase separation or intermix between two macro-phases. This result demonstrates that the R-110 film exhibits a well dispersed phase separation or better intermixing of P3HT and PCBM macro-scale components. The relative crystallinity or molecular aggregation is represented by the comparison of absorption spectra rather than AFM image herein. This result does provide strong evidence that the early crystallization mechanism of film controlled by R2R drying temperature is a critical factor to control the desired morphology of slot-die coated films. To probe the photoelectrical characteristics of these devices, the *J–V* curves in the dark for these devices are shown in Fig. 10. The devices treated with R-oven (drying process) shows a better rectification compared with the devices treated with A-oven (annealing process). In addition, the devices treated with R-oven have a smaller leakage current at negative voltages than that treated with A-oven. Also, these results provide evidences to support our hypothesis about the morphological control of drying and annealing processes correlated to the performance.

The drying process during the film formation from the wet state to dry state, evolving the solvent evaporation, high mobility and molecular ordering over large distances, is fundamentally different from the general post-drying treatments. The post drying treatments provide the less but stronger interaction between the densely packed solid components. The result indicates that the nucleation and initial growth kinetics in the drying process govern the final crystallization quality [43]. B. Schmidt–Hansberg's group studied the morphology controlled by the drying process for the blade-coated P3HT:PCBM film on the glass substrate. They consistently showed that P3HT aggregation (or ordering; UV–vis absorption) increases with the decrease of drying temperature. However, their work showed that the PCE increases with the decrease of drying temperature due to formation of the fine phase-separated morphology.

The hypothesis proposed to explain the relationship among the processing-structure-performance observed herein (the slow

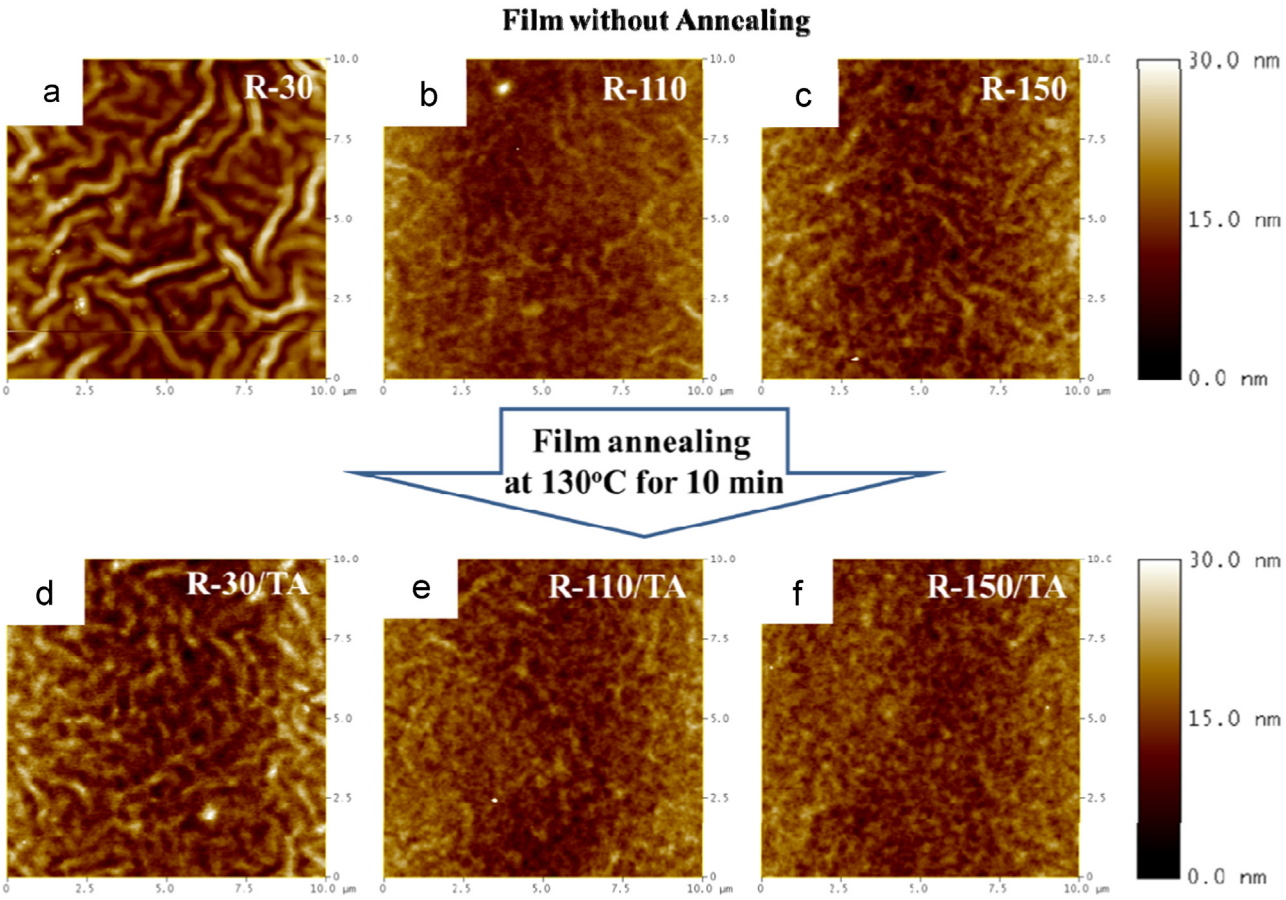

Fig. 6. Topographic AFM images of the active layers treated with R2R oven (R-oven) at (a) 30, (b) 110 and (c) 150 °C for 30 s. The corresponding films treated with a further thermal annealing process at 130 °C for 10 min are shown in (d), (e) and (f), respectively.

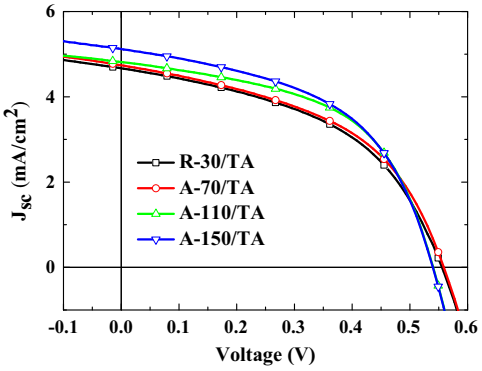

Fig. 7. *J–V* curves of devices based on the active layer prepared by o-xylene and different thermal treatment in the ambient oven.

drying at ~RT leads to a larger scale phase-separated structure and thus reduce the PCE) is based on two factors scarcely discussed: (1) there is a strong stress distribution (or stress field) within the wet film on the R2R flexible PET substrate during the solvent evaporation [17,30] and (2) the used drying temperature is greater than the corresponding glass transition temperature for the blends [54] (> 40 °C). The stress field in the solution state may reduce the polymer-fullerene interaction. The stress effect would lead to a larger P3HT:PCBM phase-separated structure. Concurrently, the higher drying temperature (> 40 °C) can provide more molecular mobility. It may be favorable to recover the destructive polymer-fullerene interaction and thus suppress the formation of such as larger scale phase-separated structure. Therefore, the fine phase-separated structure and favorable BHJ structure occurred at 110 °C (the optimum drying temperature). At the drying temperature of 150 °C, the solvent rapidly evaporates

Table 3
Photovoltaic characterization of devices under various thermal treatments by ambient oven. The photoactive layer of these devices was obtained from host solvent of o-xylene. The device area is 0.3 (1 × 0.3) cm^2, and the data are averaged over 20 devices.

Treatment	J_{sc} (mA/cm^2)	V_{oc} (V)	FF (%)	PCE_{avg} (%)	PCE_{best} (%)
A-70	4.935 ± 0.175	0.547 ± 0.012	47.067 ± 0.451	1.27 ± 0.036	1.31
A-110	4.691 ± 0.145	0.533 ± 0.007	50.167 ± 2.401	1.26 ± 0.111	1.38
A-150	4.985 ± 0.143	0.54 ± 0.004	50.533 ± 1.15	1.36 ± 0.053	1.40

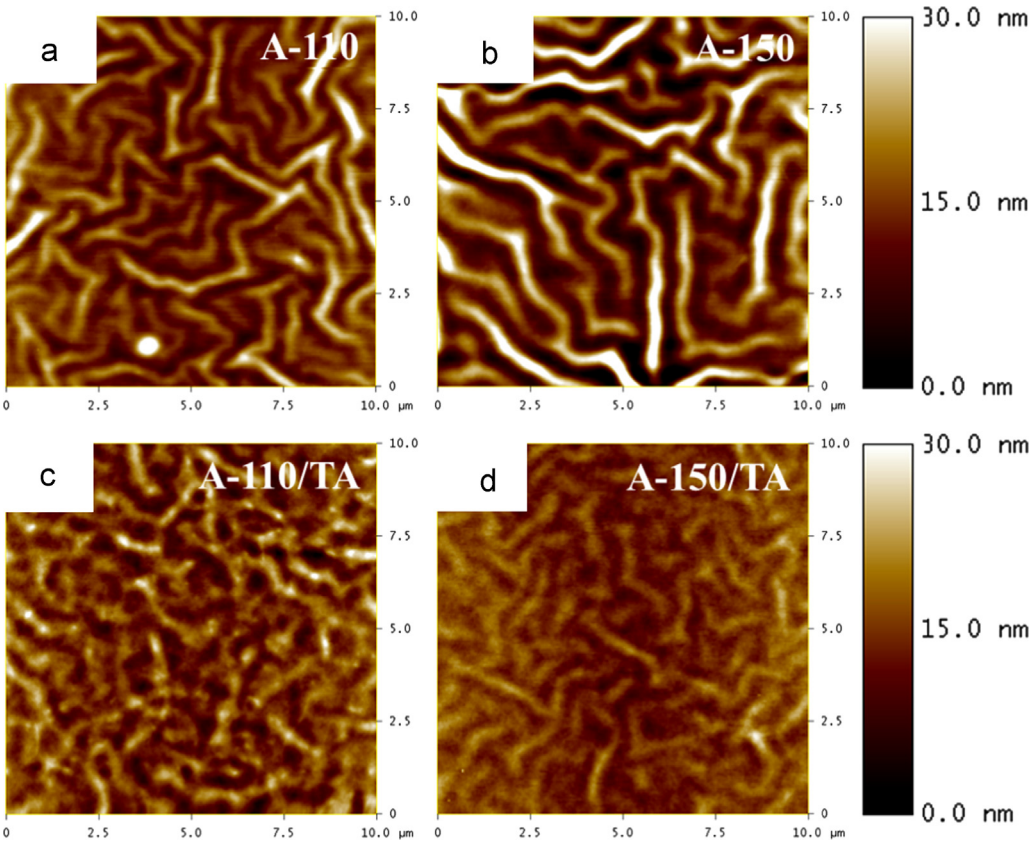

Fig. 8. Topographic AFM images of the active layers treated with ambient oven (A-oven) at (a) 110 and (b) 150 °C for 30 s. The corresponding films treated with a further thermal annealing process at 130 °C for 10 min are shown in (c) and (d), respectively.

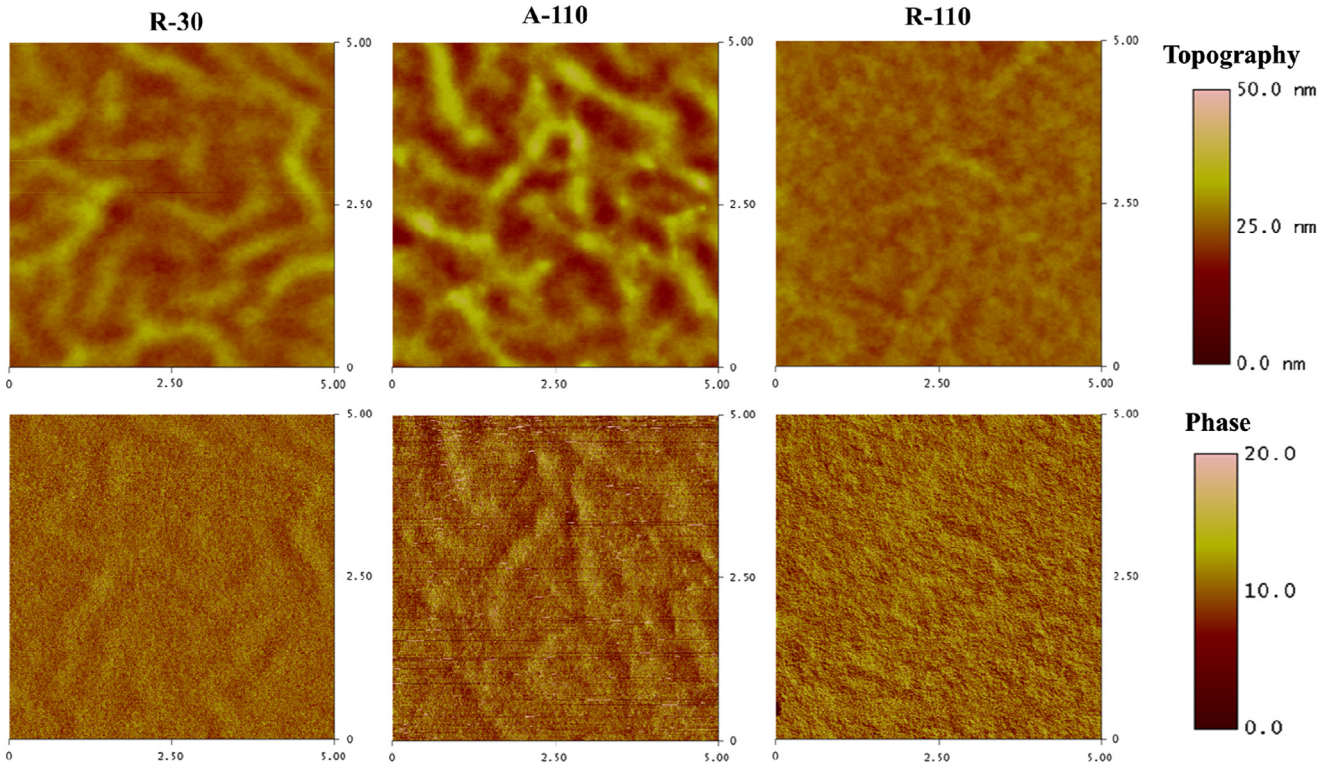

Fig. 9. Topographic AFM images and corresponding phase images of active layer treated with different thermal treatment.

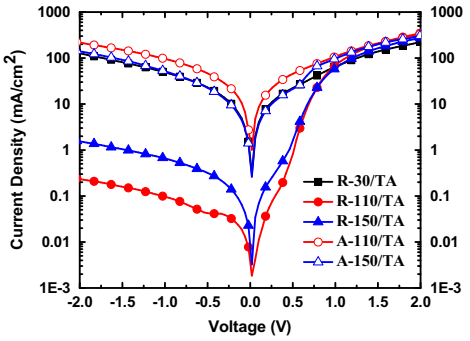

Fig. 10. Dark *J–V* curves of devices with various thermal treatments.

and part of P3HT crystallites is produced at the almost same time. These P3HT crystallites increase and grow due to the thermal annealing effect of enough high temperature [41] although it is during drying step. The crystallinity of the R-150 and R-150/TA film is slightly higher than that of R-110 and R-100/TA films, also being evidenced by the absorption spectra (Fig. 4). Therefore, the J_{sc} of the device based on R-150/TA film is higher than that based on the R-110/TA film (Tables 1 and 2). On the other hand, the growth of P3HT crystallites could retard the formation of fine phase separation because of the mutual competition between P3HT and PCBM phases [38, 41]. Hence, the fine phase-separated BHJ structure occurs at the intermediate temperature (i.e., 110 °C) and leads to a high fill factor and thus PCE. However, AFM cannot identify the little discrepancy between BHJ structure of R-110 and R150 film.

4. Conclusions

This study demonstrates that the early polymer crystallization step during transformation of the wet active layer into solid-sate film in the R2R coated process is critical to control the morphological evolution to the optimum BHJ structure. The early crystallization step can be tuned by the parameters of drying process. The complete crystallization step forming the final BHJ structure can be tuned by the thermal annealing. This study provides the insight into the understanding of how the drying and annealing processes affect the morphological evolution correlated to the performance improvement. We show that a significant improvement in performance of inverted PSCs can be achieved by the control in the drying process. Moreover, o-xylene solvent as a halogen-free solvent was successfully incorporated to the drying process for improving the performance of R2R slot-die coated inverted solar cells.

References

[1] R.R. Søndergaard, M. Hösel, F.C. Krebs, Roll-to-Roll fabrication of large area functional organic materials, J. Polym. Sci. Part B: Polym. Phys. 51 (2013) 16–34.

[2] N. Espinosa, M. Hösel, D. Angmo, F.C. Krebs, Solar cells with one-day energy payback for the factories of the future, Energy Environ. Sci. 5 (2012) 5117–5132.

[3] T.D. Nielsen, C. Cruickshank, S. Foged, J. Thorsen, F.C. Krebs, Business, market and intellectual property analysis of polymer solar cells, Sol. Energy Mater. Sol. Cells 94 (2010) 1553–1571.

[4] X. Gong, T. Yang, M. Wang, C. Duan, X. Hu, J. Peng, F. Huang, Inverted polymer solar cells with 8.4% efficiency by conjugated polyelectrolyte, Energy Environ. Sci. 5 (2012) 8208–8214.

[5] Y. Liu, J. Zhao, Z. Li, C. Mu, W. Ma, H. Hu, K. Jiang, H. Lin, H. Ade, H. Yan, Aggregation and morphology control enables multiple cases of high-efficiency polymer solar cells, Nat. Commun. 5 (2014) 5293.

[6] C.-C. Chen, W.-H. Chang, K. Yoshimura, K. Ohya, J. You, J. Gao, Z. Hong, Y. Yang, An Efficient Triple-Junction Polymer Solar Cell Having a Power Conversion Efficiency Exceeding 11%, Adv. Mater. 26 (2014) 5670–5677.

[7] J. You, L. Dou, K. Yoshimura, T. Kato, K. Ohya, T. Moriarty, K. Emery, C.C. Chen, J. Gao, G. Li, Y. Yang, A polymer tandem solar cell with 10.6% power conversion efficiency, Nat. Commun. 4 (2013) 1446.

[8] J. You, C.-C. Chen, Z. Hong, K. Yoshimura, K. Ohya, R. Xu, S. Ye, J. Gao, G. Li, Y. Yang, 10.2% power conversion efficiency polymer tandem solar cells consisting of two identical sub-cells, Adv. Mater. 25 (2013) 3973–3978.

[9] W. Li, A. Furlan, K.H. Hendriks, M.M. Wienk, R.A.J. Janssen, Efficient tandem and triple-junction polymer solar cells, J. Am. Chem. Soc. 135 (2013) 5529–5532.

[10] H.-J. Lee, H.-P. Kim, H.-M. Kim, J.-H. Youn, D.-H. Nam, Y.-G. Lee, J.-G. Lee, A. Rb Mohd Yusoff, J. Jang, Solution processed encapsulation for organic photovoltaics, Sol. Energy Mater. Sol. Cells 111 (2013) 97–101.

[11] S.W. Heo, E.J. Lee, K.W. Seong, D.K. Moon, Enhanced stability in polymer solar cells by controlling the electrode work function via modification of indium tin oxide, Sol. Energy Mater. Sol. Cells 115 (2013) 123–128.

[12] M. Jørgensen, K. Norrman, S.A. Gevorgyan, T. Tromholt, B. Andreasen, F. C. Krebs, Stability of polymer solar cells, Adv. Mater. 24 (2012) 580–612.

[13] R. Søndergaard, M. Hösel, D. Angmo, T.T. Larsen-Olsen, F.C. Krebs, Roll-to-roll fabrication of polymer solar cells, Mater. Today 15 (2012) 36–49.

[14] Y.-C. Huang, H.-C. Chia, C.-M. Chuang, C.-S. Tsao, C.-Y. Chen, W.-F. Su, Facile hot solvent vapor annealing for high performance polymer solar cell using spray process, Sol. Energy Mater. Sol. Cells 114 (2013) 24–30.

[15] M. Schrödner, S. Sensfuss, H. Schache, K. Schultheis, T. Welzel, K. Heinemann, R. Milker, J. Marten, L. Blankenburg, Reel-to-reel wet coating by variation of solvents and compounds of photoactive inks for polymer solar cell production, Sol. Energy Mater. Sol. Cells 107 (2012) 283–291.

[16] C. Koidis, S. Logothetidis, S. Kassavetis, C. Kapnopoulos, P.G. Karagiannidis, D. Georgiou, A. Laskarakis, Effect of process parameters on the morphology and nanostructure of roll-to-roll printed P3HT:PCBM thin films for organic photovoltaics, Sol. Energy Mater. Sol. Cells 112 (2013) 36–46.

[17] S. Hong, J. Lee, H. Kang, K. Lee, Slot-die coating parameters of the low-viscosity bulk-heterojunction materials used for polymer solarcells, Sol. Energy Mater. Sol. Cells 112 (2013) 27–35.

[18] J. Liu, S. Shao, G. Fang, B. Meng, Z. Xie, L. Wang, High-efficiency inverted polymer solar cells with transparent and work-function tunable MoO_3-Al composite film as cathode buffer layer, Adv. Mater. 24 (2012) 2774–2779.

[19] Z. Liang, Q. Zhang, O. Wiranwetchayan, J. Xi, Z. Yang, K. Park, C. Li, G. Cao, Effects of the morphology of a ZnO buffer layer on the photovoltaic performance of inverted polymer solar cells, Adv. Funct. Mater. 22 (2012) 2194–2201.

[20] B. Park, J.C. Shin, C.Y. Cho, Water-processable electron-collecting layers of a hybrid poly(ethylene oxide): Caesium carbonate composite for flexible inverted polymer solar cells, Sol. Energy Mater. Sol. Cells 108 (2013) 1–8.

[21] Y.-J. Kang, K. Lim, S. Jung, D.-G. Kim, J.-K. Kim, C.-S. Kim, S.H. Kim, J.-W. Kang, Spray-coated ZnO electron transport layer for air-stable inverted organic solar cells, Sol. Energy Mater. Sol. Cells 96 (2012) 137–140.

[22] A. Lange, W. Schindler, M. Wegener, K. Fostiropoulos, S. Janietz, Inkjet printed solar cell active layers prepared from chlorine-free solvent systems, Sol. Energy Mater. Sol. Cells 109 (2013) 104–110.

[23] M. Välimäki, P. Apilo, R. Po, E. Jansson, A. Bernardi, M. Ylikunnari, M. Vilkman, G. Corso, J. Puustinen, J. Tuominen, J. Hast, R2R-printed inverted OPV modules – towards arbitrary patterned designs, Nanoscale 7 (2015) 9570–9580.

[24] C. Kapnopoulos, E.D. Mekeridis, L. Tzounis, C. Polyzoidis, A. Zachariadis, S. Tsimikli, C. Gravalidis, A. Laskarakis, N. Vouroutzis, S. Logothetidis, Fully gravure printed organic photovoltaic modules: A straightforward process with a high potential for large scale production, Sol. Energy Mater. Sol. Cells 144 (2016) 724–731.

[25] H.-C. Cha, Y.-C. Huang, F.-H. Hsu, C.-M. Chuang, D.-H. Lu, C.-W. Chou, C.-Y. Chen, C.-S. Tsao, Performance improvement of large-area roll-to-roll slot-die-coated inverted polymer solar cell by tailoring electron transport layer, Sol. Energy Mater. Sol. Cells 130 (2014) 191–198.

[26] J.E. Carlé, T.R. Andersen, M. Helgesen, E. Bundgaard, M. Jørgensen, F.C. Krebs, A laboratory scale approach to polymer solar cells using one coating/printing machine, flexible substrates, no ITO, no vacuum and no spincoating, Sol. Energy Mater. Sol. Cells 108 (2013) 126–128.

[27] D. Angmo, S.A. Gevorgyan, T.T. Larsen-Olsen, R.R. Søndergaard, M. Hösel, M. Jørgensen, R. Gupta, G.U. Kulkarni, F.C. Krebs, Scalability and stability of very thin, roll-to-roll processed, large area, indium-tin-oxide free polymer solar cell modules, Org. Electron. 14 (2013) 984–994.

[28] M. Hösel, F.C. Krebs, Large-scale roll-to-roll photonic sintering of flexo printed silver nanoparticle electrodes, J. Mater. Chem. 22 (2012) 15683–15688.

[29] N. Espinosa, F.O. Lenzmann, S. Ryley, D. Angmo, M. Hösel, R.R. Søndergaard, D. Huss, S. Dafinger, S. Gritsch, J.M. Kroon, M. Jørgensen, F.C. Krebs, OPV for mobile applications: an evaluation of roll-to-roll processed indium and silver free polymer solar cells through analysis of life cycle, cost and layer quality using inline optical and functional inspection tools, J. Mater. Chem. A 1 (2013) 7037–7049.

[30] F. Jakubka, M. Heyder, F. Machui, J. Kaschta, D. Eggerath, W. Lövenich, F. C. Krebs, C.J. Brabec, Determining the coating speed limitations for organic photovoltaic inks, Sol. Energy Mater. Sol. Cells 109 (2013) 120–125.

[31] T.T. Larsen-Olsen, B. Andreasen, T.R. Andersen, A.P.L. Böttiger, E. Bundgaard, K. Norrman, J.W. Andreasen, M. Jørgensen, F.C. Krebs, Simultaneous multilayer

formation of the polymer solar cell stack using roll-to-roll double slot-die coating from water, Sol. Energy Mater. Sol. Cells 97 (2012) 22–27.
[32] G.D. Spyropoulos, P. Kubis, N. Li, D. Baran, L. Lucera, M. Salvador, T. Ameri, M. Voigt, F.C. Krebs, C.J. Brabec, Flexible organic tandem solar modules with 6% efficiency: combining roll-to-roll compatible processing with high geometric fill factors, Energy Environ. Sci. 7 (2014) 3284–3290.
[33] L. Lucera, P. Kubis, F.W. Fecher, C. Bronnbauer, M. Turbiez, K. Forberich, T. Ameri, H.-J. Egelhaaf, C.J. Brabec, Guidelines for closing the efficiency gap between hero solar cells and roll-to-roll printed modules, Energy Technol. 3 (2015) 373–384.
[34] L. Wengeler, M. Schmitt, K. Peters, P. Scharfer, W. Schabel, Comparison of large scale coating techniques for organic and hybrid films in polymer based solar cells, Chem. Eng. Process. : Process. Intensif. 68 (2013) 38–44.
[35] M. Helgesen, J.E. Carlé, F.C. Krebs, Slot-die coating of a high performance copolymer in a readily scalable roll process for polymer solar cells, Adv. Energy Mater. 3 (2013) 1664–1669.
[36] J.E. Carlé, M. Helgesen, N.K. Zawacka, M.V. Madsen, E. Bundgaard, F.C. Krebs, A comparative study of fluorine substituents for enhanced stability of flexible and ITO-free high-performance polymer solar cells, J. Polym. Sci. Part B: Polym. Phys. 52 (2014) 893–899.
[37] H.-C. Liao, C.-S. Tsao, T.-H. Lin, C.-M. Chuang, C.-Y. Chen, U.S. Jeng, C.-H. Su, Y.-F. Chen, W.-F. Su, Quantitative nanoorganized structural evolution for a high efficiency bulk heterojunction polymer solar cell, J. Am. Chem. Soc. 133 (2011) 13064–13073.
[38] H.-C. Liao, C.-S. Tsao, T.-H. Lin, M.-H. Jao, C.-M. Chuang, S.-Y. Chang, Y.-C. Huang, Y.-T. Shao, C.-Y. Chen, C.-J. Su, U.S. Jeng, Y.-F. Chen, W.-F. Su, Nanoparticle-tuned self-organization of a bulk heterojunction hybrid solar cell with enhanced performance, ACS Nano 6 (2012) 1657–1666.
[39] Y.-C. Huang, C.-S. Tsao, C.-M. Chuang, C.-H. Lee, F.-H. Hsu, H.-C. Cha, C.-Y. Chen, T.-H. Lin, C.-J. Su, U.S. Jeng, W.-F. Su, Small- and wide-angle X-ray scattering characterization of bulk heterojunction polymer solar cells with different fullerene derivatives, J. Phys. Chem. C 116 (2012) 10238–10244.
[40] C.-Y. Chen, C.-S. Tsao, Y.-C. Huang, H.-W. Liu, W.-Y. Chiu, C.-M. Chuang, U. S. Jeng, C.-J. Su, W.-R. Wu, W.-F. Su, L. Wang, Mechanism and control of structural evolution of polymer solar cell from bulk heterojunction to thermally unstable hierarchical structure, Nanoscale 5 (2013) 7629–7638.
[41] E. Verploegen, R. Mondal, C.J. Bettinger, S. Sok, M.F. Toney, Z. Bao, Effects of thermal annealing upon the morphology of polymer–fullerene blends, Adv. Funct. Mater. 20 (2010) 3519–3529.
[42] H.-C. Liao, C.-S. Tsao, Y.-T. Shao, S.-Y. Chang, Y.-C. Huang, C.-M. Chuang, T.-H. Lin, C.-Y. Chen, C.-J. Su, U.S. Jeng, Y.-F. Chen, W.-F. Su, Bi-hierarchical nanostructures of donor-acceptor copolymer and fullerene for high efficient bulk heterojunction solar cells, Energy Environ. Sci. 6 (2013) 1938–1948.
[43] Z. Zang, A. Nakamura, J. Temmyo, Single cuprous oxide films synthesized by radical oxidation at low temperature for PV application, Opt. Expr. 21 (2013) 11448–11456.
[44] B. Schmidt-Hansberg, M. Sanyal, M.F.G. Klein, M. Pfaff, N. Schnabel, S. Jaiser, A. Vorobiev, E. Müller, A. Colsmann, P. Scharfer, D. Gerthsen, U. Lemmer, E. Barrena, W. Schabel, Moving through the phase diagram: morphology formation in solution cast polymer–fullerene blend films for organic solar cells, ACS Nano 5 (2011) 8579–8590.
[45] M. Sanyal, B. Schmidt-Hansberg, M.F.G. Klein, A. Colsmann, C. Munuera, A. Vorobiev, U. Lemmer, W. Schabel, H. Dosch, E. Barrena, In Situ X-Ray study of drying-temperature influence on the structural evolution of bulk-heterojunction polymer-fullerene solar cells processed by doctor-blading, Adv. Energy Mater. 1 (2011) 363–367.
[46] B. Schmidt-Hansberg, M. Sanyal, N. Grossiord, Y. Galagan, M. Baunach, M.F. G. Klein, A. Colsmann, P. Scharfer, U. Lemmer, H. Dosch, J. Michels, E. Barrena, W. Schabel, Investigation of non-halogenated solvent mixtures for high throughput fabrication of polymer–fullerene solar cells, Sol. Energy Mater. Sol. Cells 96 (2012) 195–201.
[47] G. Li, Y. Yao, H. Yang, V. Shrotriya, G. Yang, Y. Yang, Solvent annealing effect in polymer solar cells based on poly(3-hexylthiophene) and methanofullerenes, Adv. Funct. Mater. 17 (2007) 1636–1644.
[48] S. Chen, W. Zeng, X. Su, J. Wang, D. Wang, H. Zhang, Effect of preparation parameters on performance of P3HT: PCBM solar cells, Mater. Sci. Semicond. Process. 39 (2015) 441–446.
[49] Z. Hu, J. Zhang, L. Huang, J. Sun, T. Zhang, H. He, J. Zhang, H. Zhang, Y. Zhu, Natural drying effect on active layer for achieving high performance in polymer solar cells, Renew. Energy 74 (2015) 11–17.
[50] Y.-C. Huang, Y.-C. Liao, S.-S. Li, M.-C. Wu, C.-W. Chen, W.-F. Su, Study of the effect of annealing process on the performance of P3HT/PCBM photovoltaic devices using scanning-probe microscopy, Sol. Energy Mater. Sol. Cells 93 (2009) 888–892.
[51] M.-S. Kim, B.-G. Kim, J. Kim, Effective variables to control the fill factor of organic photovoltaic cells, ACS Appl. Mater. Interfac. 1 (2009) 1264–1269.
[52] B. Qi, J. Wang, Fill factor in organic solar cells, Phys. Chem. Chem. Phys. 15 (2013) 8972–8982.
[53] W. Ma, J.Y. Kim, K. Lee, A.J. Heeger, Effect of the molecular weight of poly(3-hexylthiophene) on the morphology and performance of polymer bulk heterojunction solar cells, Macromol. Rapid Commun. 28 (2007) 1776–1780.
[54] J. Zhao, A. Swinnen, G. Van Assche, J. Manca, D. Vanderzande, B. Van Mele, Phase diagram of P3HT/PCBM blends and its implication for the stability of morphology, J. Phys. Chem. B 113 (2009) 1587–1591.